BBAA VI International Colloquium on:
Bluff Bodies Aerodynamics & Applications
Milano, Italy, July, 20–24 2008

WIND INDUCED DYNAMICS OF A PRISMATIC SLENDER BUILDING WITH 1:3 RECTANGULAR SECTION

Alberto Zasso*, Aly Mousaad Aly*, Lorenzo Rosa* and Gisella Tomasini*

*Politecnico di Milano, Campus Bovisa, Department of Mechanical Engineering
Via La Masa 34, 20156 Milano, Italy
e-mails: alberto.zasso@polimi.it, aly.mousaad@polimi.it,
lorenzo.rosa@polimi.it, gisella.tomasini@polimi.it

Keywords: Aerodynamics, Damping, FEM, Rectangular Prism, Tall Buildings, Wind Tunnel Testing.

Abstract: *This paper presents a detailed study to investigate the aerodynamics and dynamic behavior of a slender tall building with rectangular cross-section. The building has the shape of rectangular prism which is a common shape of buildings, bridge decks and bridge towers. Both 2D sectional and 3D rigid models are used to experimentally understand the wind flow around the prism. The 2D sectional model was used to further the understanding of the effect of the wind attack angle and the galloping instability of the prism. 3D rigid model was used to study both effects of turbulence and the wind attack angle on such instability. Wind loads obtain from surface pressure integration on the 3D model are used later with Finite Element Modeling (FEM) of the full scale building for dynamic response prediction. In this study, it has been shown that the effect of turbulence and the wind attack angle is a key point that affects very much on both stability and dynamic responses (displacements and accelerations) of the tower. The main objective of the present study is to further the understanding of wind effects on tall buildings and the behavior of high-rise structures under wind conditions by means of wind tunnel testing and FEM in order to apply such knowledge to design.*

1 INTRODUCTION

Developments in structural materials and design technology in civil engineering have led to designs that satisfy strength requirements but are often very flexible. These flexibilities lead to unfavorable dynamic responses that may affect on the structural serviceability and occupants comfort when the structure is subjected to dynamic loads like strong winds and earthquakes.

Traditionally, responses of these structures can be evaluated analytically using some codes and formulas [1, 2, 3, 4, 5, 6]. However, these standards provide little guidance for the critical across-wind and torsional responses. This is partially attributed to the fact that the across-wind and torsional responses, unlike the along-wind, result mainly from the aerodynamic pressure fluctuations in the separated shear layers and the wake flow fields, which have prevented, to date, any acceptable direct analytical relation to the oncoming velocity fluctuations [7]. Also, these methods have its limitations especially when some other tall structures exist in the vicinity of the building under consideration. Moreover, responses are restricted to some few modes and the process of evaluating such response depends on much assumption. Wind tunnel measurements and finite element modeling (FEM) of the structures are an effective alternative for determining these responses.

Wind tunnel tests are recommended for acquiring wind loads on the surface of the building under consideration. FEM technique provides a detailed in depth description of the dynamic behavior of the structure. Three dimensional FEM is favorable in predicting the responses of a building as it can combine instantaneously the torsional response with the two in-plane lateral responses considering much higher modes. Also, it produces a mesh on the outer surface of the building by which one can use the pressure integration technique to distribute extensively the external pressure forces on the outer surface of the building [8].

This paper presents a detailed study to investigate the influences of incident wind direction, upstream terrain conditions and interferences from the surroundings on wind responses of a tall prismatic building. The rectangular prism is a common shape of buildings, bridge decks and bridge towers. In the theoretical formulation, dynamic equations of the structure are introduced by finite element analysis, and then a solution procedure for a set of ordinary differential equations are considered by combining the first six vibrational modes. It has been shown that the effect of turbulence and the wind attack angle is a key point that affects very much on both stability and dynamic responses of the tower. The effect of the wind attack angle is very important as both root mean square (rms) and peak responses may occur at wind attack angles rather than $0deg$ and $90deg$. Such effects cannot easily predicted by current codes. The main objective of this study is to further the understanding of wind effects on tall buildings and the behavior of high-rise structures under wind conditions by means of wind tunnel tests in order to apply such knowledge to design as the tower still in its preliminary design stages.

2 AERODYNAMICS OF THE RECTANGULAR PRISM

In the year 1934, Prandtl & Tiejens provided the definition of a “bluff-body”. They wrote, Ref. [9]: *The simple relations just outlined (invariability of drag coefficients with change in Reynolds’ number) are practically true for bodies where the total drag consists almost exclusively of pressure drag and where the geometry of the flow, in particular the breaking away of the fluid, is determined by sharp edges as, for instance, with a plate perpendicular to the direction of the flow*. This statement provides that if a bluff-body has sharp edges, for which the separation point is defined at the leading edge, there are no Reynolds number effects on the aerodynamics of the body. As a result, even if the Reynolds number similitude in wind tunnel

tests on rectangular prism with sharp edges is not satisfied, the aerodynamic force coefficients on the model and on the prototype will probably the same. ($Re \cong 10^3 - 10^4$).

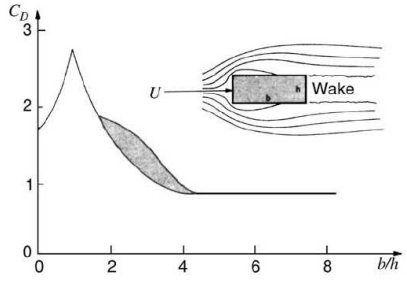

Figure 1: Drag coefficient versus elongation ratio B/D of a rectangular prism with sharp edges, [10].

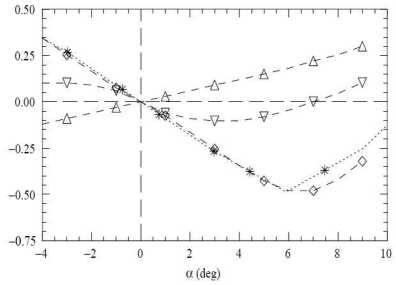

Figure 2: Variation of C_L with angle of attack and turbulence level, for a $B/D = 2$ rectangular prism with sharp edges, [14]. $\triangledown$: $I_u = 5\%$; $\triangle$: $I_u = 11\%$, $\diamond, *$: *smooth-flow*.

Given Prandtl & Tiejens assumption, the impossibility of doing tests at Reynolds numbers equal to full-size and that tests at low Reynolds reduces the cost of wind tunnel operation, the Reynolds number similitude was many times "relaxed" in the past, doing investigation on civil structures at low Reynolds. However, recent full-scale measurements, data obtained from large low-speed wind tunnel and a series of studies from Simiu and Scanlan, have disputed the assumption made by Prandtl & Tiejens. Fig. 1 presented by Simiu & Scanlan collects data from different sources regarding the drag coefficient, C_D, versus the elongation ratio B/D of rectangular prisms with sharp edges. The figure shows that if the prism has a $B/D \cong 1$ or $B/D > 4$ the value of the C_D is unique. On the other hand, there is a grey zone for the elongation ratios $2 < B/D < 4$ where the C_D shows some dispersions, indication of a sensitivity to the Reynolds number.

It has been established that this dispersion is related to a possible presence of a reattachment point on the sides of the prism. The possibility of reattachment of the boundary layer, forced to separate at the windward corners, depends on many parameters such the elongation ratio, edge geometry, turbulence and angle of attack. The presence, and the position, of this reattachment point must be considered because it plays an important role on the aerodynamics of rectangular prisms, [11, 12, 13, 14].

Figure 2 reports lift coefficients, C_L, for a $B/D = 2$ rectangular prism with sharp edges. This coefficient is very sensitive to the angle of attack and the level of turbulence of the incoming flow: in low-turbulence condition the section shows a C_L trend with negative slope, dangerous because potential for galloping dynamic instability, [15]. However, at higher turbulence, the slope becomes positive and the instability doesn't occur. The behavior of prisms in this B/D range must be considered in the design stage as their aerodynamics is strongly affected by flow conditions [12]. Among all the parameters, the lift coefficient, C_L, is the most sensitive parameter to the angle of attack and the level of turbulence in the incoming flow.

3 WIND TUNNEL TESTS ON A 2D SECTIONAL MODEL

2D sectional and 3D rigid models were used for wind tunnel tests. The experiment was carried out in the Boundary Layer Test Section of the Wind Tunnel at Politecnico di Milano, that is $4m$ height, $14m$ width and $36m$ length. The building tower considered in this study

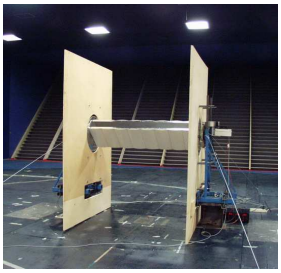

Figure 3: The 2D sectional model on the dynamometric balance.

Figure 4: 3D rigid model in SF configuration.

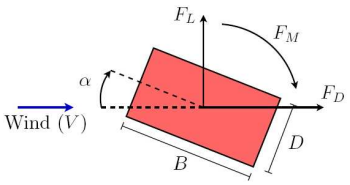

Figure 5: The symbols used for showing the results.

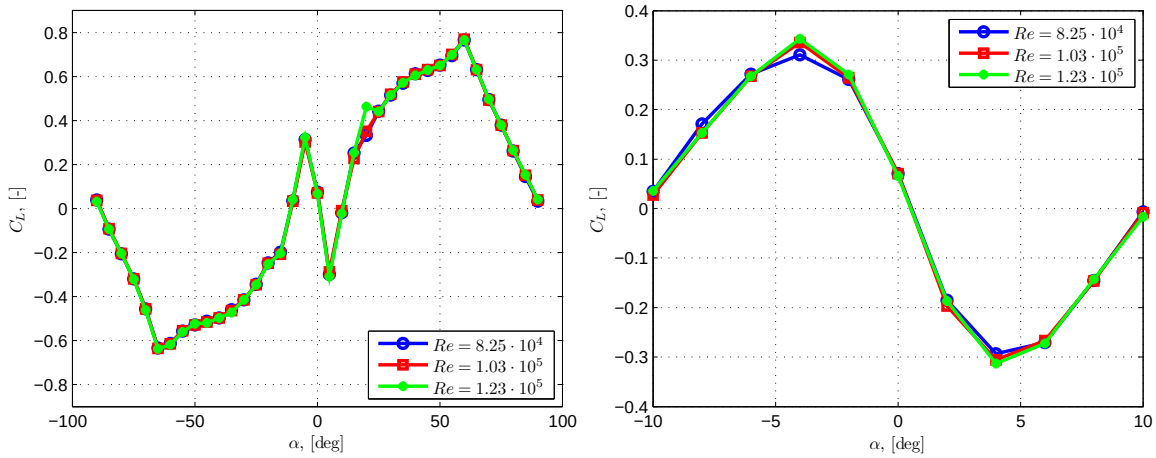

(a) 2D model, SF, $-90 < \alpha < +90$

(b) 2D model, SF, $-10 < \alpha < +10$

Figure 6: Trend of the lift coefficient, C_L, versus the wind attack angle, α

represents a common high-rise building with geometry very similar to a regular rectangular prism.

The 2D sectional model was used to evaluate the two dimensional smooth flow (SF) behavior around the prism. In this test configuration, the boundary layer thickness is about 0.2 m and the turbulence intensity, I_u, outside the boundary layer is lower than 2% (see Fig. 7). For the first analysis it was hanged by a multicomponent load cell at each side; the cells were mounted on a mechanism driven by a motor allowing $360deg$ rotation of the entire model as shown on Fig. 3. In this manner it was possible to change the angle of attack and to measure for every configuration the drag, lift, and moment force components.

In the first part of the research project the rigidly supported 2D sectional model was tested in low-turbulence flow with an angle of attack $\alpha = \pm 90deg$ (Fig. 3). Figure 6 gives the trend of the lift coefficient, C_L, versus the wind attack angle, α (the conventions used for showing the results are presented in Fig. 5). It is shown on the figure that there is a sharp change in the C_L values from positive to negative over a small variations in the wind attack angle ($-4 < \alpha < 4$). Such sharp sudden changes may show potential for galloping instability, based on Den Hartog criteria, Eq. (1) given their negative slope of C_L versus α at 0deg, [15].

$$\frac{\partial C_L}{\partial \alpha} + C_D \leq 0 \tag{1}$$

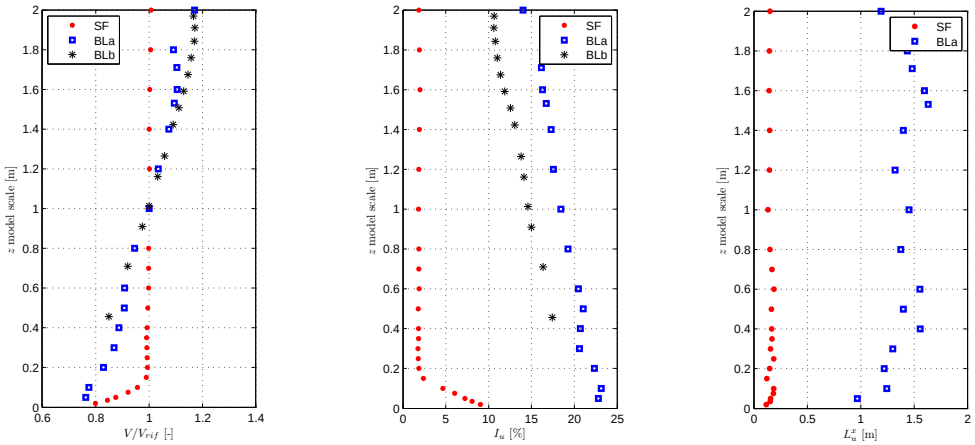

(a) V/V_{rif} profile. (b) I_u profile. (c) L_u^x profile.

Figure 7: Flow characteristics during the tests: SF, BLa and BLb configurations.

4 WIND TUNNEL TESTS ON 3D RIGID MODEL

4.1 Test arrangements

In order to deeply investigate the aerodynamic behavior of the prism and to obtain surface pressure measurements, that is necessary for predicting wind loads for the FEM model, a rigid 3D model of the tower was used. The 3D model is indicated on Fig. 4. The tower considered in this study represents a high-rise building that is to be constructed in the city of Milan, Italy. The outer dimensions of the full-scale building are $209m$ height, $57.6m$ width, and $22.5m$ depth. A rigid 3D model of the tower made of carbon fiber and geometrically scaled by 1:100 was used for wind tunnel tests. The surrounding buildings within a radius of 500 m from the center of the tower were also scaled 1:100 to be presented on the turning test table according to the type of the test configuration used. The huge dimensions of the Boundary Layer test section allows for testing civil engineering structural models with large scales (up to 1:50) with low blockage effects. The long length of the test section allows for the turbulent boundary layer to be developed properly. Passive vortex generators in the form of spires, brick and roughness elements in the shape of pyramids were used at the entrance of the test section to stimulate the growth of the boundary layer and to produce a flow with different characteristics. Two levels of turbulence intensity and integral length scale were generated, hereafter called BLa and BLb: the BLa configuration has turbulence values greater than BLb, similar to an urban site. The integral length scale in BLb configuration is about 10% lower than BLa configuration. The flow characteristic simulated in the wind tunnel are summarized in Figure 7. Two different site configurations (referred to as Config. I and Config. II) are considered in this paper, (see Fig. 8). The main objective of the wind tunnel tests is to conduct surface pressure measurements, acquired using the high speed PSI-system 8400. Pressure measurements are favorable to be used with the FEM in order to predict the responses of the tower as it can accurately distribute the wind load on the outer surface of the model [8].

4.2 Test results

Figure 9(a) shows the C_L computed for each section of the model in SF, compared with the coefficient measured on the sectional model. Line "TOT" stands for the integration of the global pressure field and represents the 3D model aerodynamic behavior. The global behavior of the

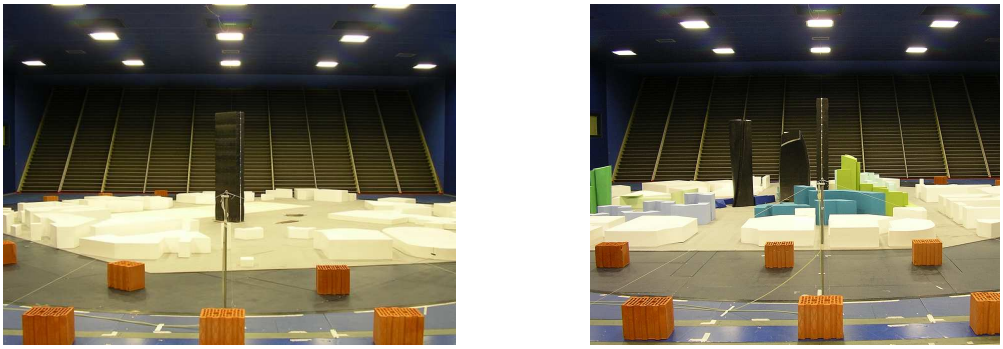

(a) Site Config. I (exp: 45deg). (b) Site Config. II (exp: 180deg).

Figure 8: Wind tunnel site configurations for the 3D rigid model tests.

sectional and the 3D model is quite similar (lines 2D and TOT), but the C_L trend changes along prism height. Figure 9(b) reports the C_L trend in turbulence flows ($I_u = 17\%$ and $L_u^x/D = 6.5$ at the reference height). The curves slope is always positive and all the model slices have a similar behavior. The role of the free-stream turbulence is to gives more energy to the flow and increases the growth rate of the shear layer: the consequence is to shorten the separation bubble. The shortening of the separation bubble length causes an earlier reattachment of the separated shear layer and a fast mean pressure recovery, that affects the lift and drag coefficients. The results is that stability of the prism is related to the turbulence level and increasing the turbulence lead to prism stability. This behavior is explained in Fig. 10 in which the pressure distribution

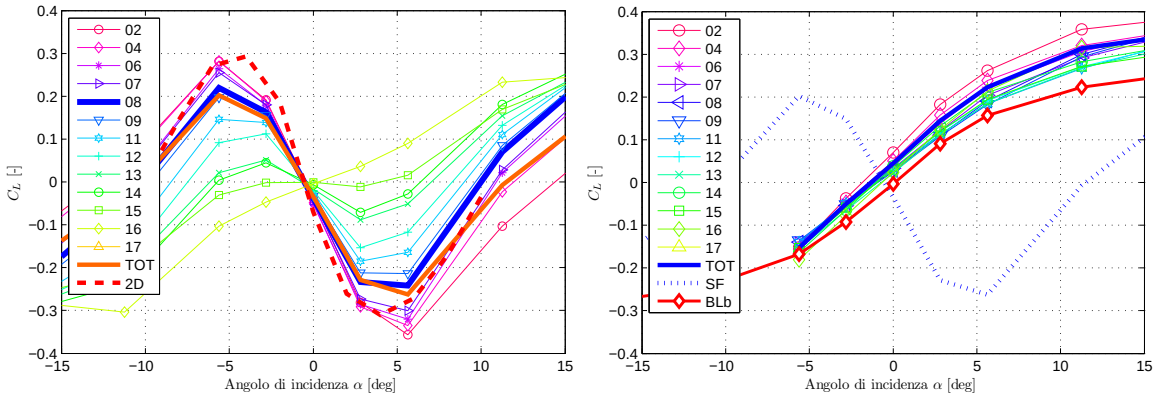

(a) 3D model, SF (b) 3D model, BLa

Figure 9: Steady aerodynamic lift force coefficient, C_L, in SF and BLa configurations. The legend, in the 3D case, shows the number of the model slice.

around section 8 (slice 8 is at about $2/3$ height of the building) and the respective lift and drag forces, obtained from the pressure integration, are illustrated. Considering this figure, it is clear the alteration of the flow pattern on the flow facing-side of the prism due to the increased turbulence and the consequent change of the lift force coefficient. A detailed study about this behavior is present in [16].

5 3D FEM OF THE TOWER

FEM of the full-scale building tower is provided in Fig. 11. Modal parameters of the FEM for the first six modes are given in Table 13. Equations of motion governing the behavior of the

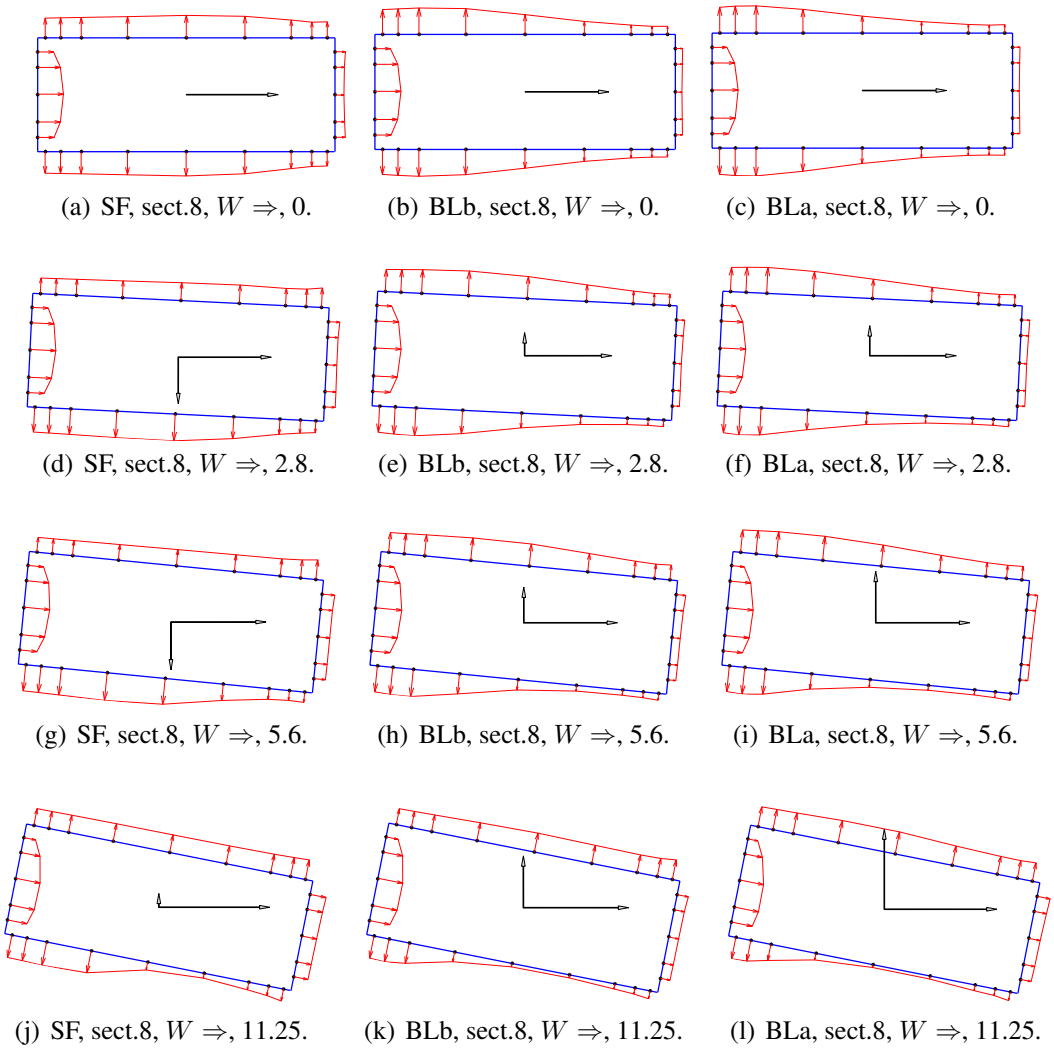

(a) SF, sect.8, $W \Rightarrow$, 0. (b) BLb, sect.8, $W \Rightarrow$, 0. (c) BLa, sect.8, $W \Rightarrow$, 0.

(d) SF, sect.8, $W \Rightarrow$, 2.8. (e) BLb, sect.8, $W \Rightarrow$, 2.8. (f) BLa, sect.8, $W \Rightarrow$, 2.8.

(g) SF, sect.8, $W \Rightarrow$, 5.6. (h) BLb, sect.8, $W \Rightarrow$, 5.6. (i) BLa, sect.8, $W \Rightarrow$, 5.6.

(j) SF, sect.8, $W \Rightarrow$, 11.25. (k) BLb, sect.8, $W \Rightarrow$, 11.25. (l) BLa, sect.8, $W \Rightarrow$, 11.25.

Figure 10: Mean pressure distribution on section 8. I_u^{SF}=1.8%, I_u^{BLb}=13%, I_u^{BLa}=17%. The arrows indicate the lift and drag forces obtained from the pressure integration. The wind comes from the left side, $W \Longrightarrow$.

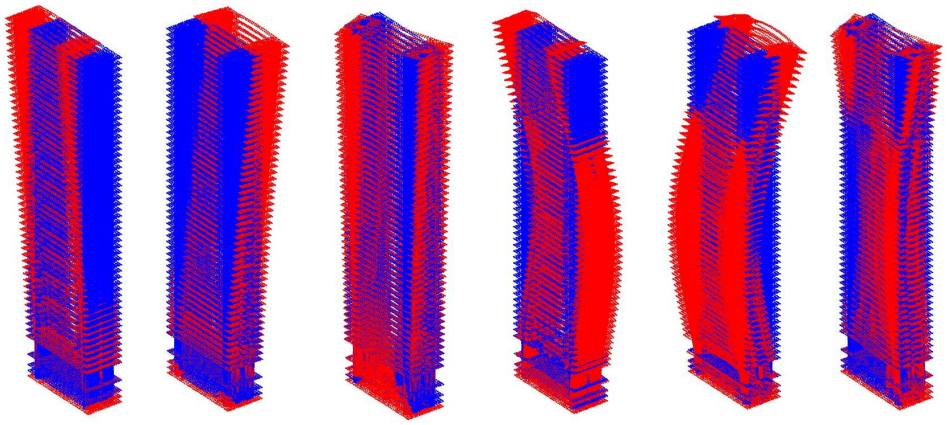

1st mode 2nd mode 3rd mode 4th mode 5th mode 6th mode

Figure 11: FEM of the building with the first six mode shapes.

structure under wind loads are

$$\mathbf{M\ddot{X}} + \mathbf{C\dot{X}} + \mathbf{KX} = \mathbf{F(t)} \tag{2}$$

where $\mathbf{X} = [\ \mathbf{x}\quad \mathbf{y}\quad \mathbf{z}\ ]^{\mathbf{T}}$ is a $(3n \times 1)$ vector and n is the number of nodes while $\mathbf{x}$, $\mathbf{y}$, and $\mathbf{z}$ are vectors of nodal displacements in *x*, *y*, and *z* directions respectively.

Time history of the pressure forces acting at each external surface node is obtained by integrating wind pressure over the corresponding effective surface area to give the three components of the force. However, forces acting on the internal nodes are obviously equal to zero. Using the first six modes given from the FEM, with the next transformation:

$$\mathbf{X} = \mathbf{\Phi q} \tag{3}$$

$$\mathbf{\Phi} = \begin{bmatrix} \phi_1(x_1) & \phi_2(x_1) & \dots & \phi_6(x_1) \\ \phi_1(x_2) & \phi_2(x_2) & \cdots & \phi_6(x_2) \\ \vdots & \vdots & \vdots & \vdots \\ \phi_1(x_n) & \phi_2(x_n) & \cdots & \phi_6(x_n) \\ \phi_1(y_1) & \phi_2(y_1) & \dots & \phi_6(y_1) \\ \phi_1(y_2) & \phi_2(y_2) & \cdots & \phi_6(y_2) \\ \vdots & \vdots & \vdots & \vdots \\ \phi_1(y_n) & \phi_2(y_n) & \cdots & \phi_6(y_n) \\ \phi_1(z_1) & \phi_2(z_1) & \dots & \phi_6(z_1) \\ \phi_1(z_2) & \phi_2(z_2) & \cdots & \phi_6(z_2) \\ \vdots & \vdots & \vdots & \vdots \\ \phi_1(z_n) & \phi_2(z_n) & \cdots & \phi_6(z_n) \end{bmatrix}, \mathbf{q} = \begin{Bmatrix} q_1 \\ q_2 \\ \vdots \\ \vdots \\ q_6 \end{Bmatrix} \tag{4}$$

where $\mathbf{\Phi}$ is $(3n \times 6)$ matrix of eigenvectors and $\mathbf{q}$ is (6×1) vector of generalized displacements. Substituting by Eq. (3) into Eq. (2) and premultiplying by $\mathbf{\Phi^T}$, one obtain

$$\mathbf{\Phi^T M \Phi \ddot{q}} + \mathbf{\Phi^T C \Phi \dot{q}} + \mathbf{\Phi^T K \Phi q} = \mathbf{\Phi^T F(t)} \tag{5}$$

By assuming the damping matrix, $\mathbf{C}$, to be a proportional damping, the above equations results into six uncoupled equations:

$$\left.\begin{aligned} m_{11}\ddot{q}_1 + c_{11}\dot{q}_1 + k_{11}q_2 &= \sum_{i=1}^{n} \phi_1(x_i)\, F_{x,i}(t) + \sum_{i=1}^{n} \phi_1(y_i)\, F_{y,i}(t) + \sum_{i=1}^{n} \phi_1(z_i)\, F_{z,i}(t) \\ &\vdots \\ m_{66}\ddot{q}_6 + c_{66}\dot{q}_6 + k_{66}q_6 &= \sum_{i=1}^{n} \phi_6(x_i)\, F_{x,i}(t) + \sum_{i=1}^{n} \phi_6(y_i)\, F_{y,i}(t) + \sum_{i=1}^{n} \phi_6(z_i)\, F_{z,i}(t) \end{aligned}\right\} \tag{6}$$

where m_{ii}, c_{ii}, and k_{ii} are generalized mass, generalized damping, and generalized stiffness of the i^{th} mode respectively. The $q_i(t)$ are then solved from each of the above equations. Simulink is used for the numerical solution of the above equations.

6 DYNAMIC RESPONSE UNDER WIND LOADS

Figures (14-16) show the displacement and acceleration responses of the top corner of the tower in both x-direction and y-direction as a function of the approaching wind angle. The

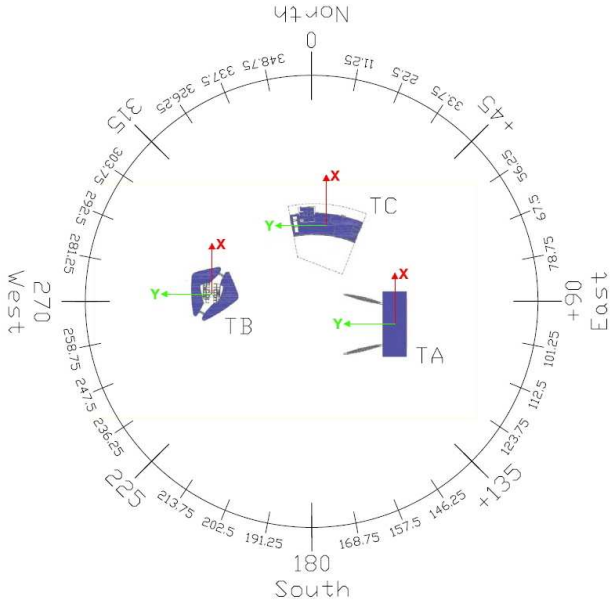

Figure 12: Wind direction for the test on the entire tower.

Mode No.	Freq.[Hz]	Modal h%
1	0.1446	0.01
2	0.1528	0.01
3	0.2545	0.01
4	0.4511	0.01
5	0.6269	0.01
6	0.8812	0.01

Figure 13: Modal parameters of the full-scale building

design wind speed is taken as 28.5 m/s which corresponds to a return period of five years. On the figures, Config. I and Config. II refer to the responses of the top corner of the tower under the site configurations indicated by Fig. 8. In this study, the terms along-wind and across-wind responses refers to the nodal responses of the top corner in x and y-directions. The response is called along-wind in one direction if it coincides or has a small shift angle with the wind load direction. Note also that, unlike many previous studies, both along-wind and across-wind responses here represents the lateral in-plane responses in addition to the torsional responses of the tower that is added instantaneously to the two lateral in-plane responses. Effect of damping on the rms-displacement and acceleration responses is studied by considering three different damping ratios (1%, 2% and 4% which is referred to as h1%, h2% and h4% respectively).

The along-wind mean displacement response in the y-direction is higher than that in the x-direction due to the fact that it is dominated by the mean wind load which is higher in the y-direction due to the rectangular cross section of the building (i.e. the drag face of the building is wider in the y-direction than that in the x-direction). However, rms-displacements and rms-accelerations along-wind in the y-direction still have significantly high values (with respect to the across-wind responses in the y-direction) when compared to those in the x-direction (across-wind responses are much higher than along-wind responses in x-direction).

Figures (15-16) show that rms-displacement responses strongly depend on the incident wind direction for both of the two configurations. It is also shown that rms-displacement responses in the across-wind direction are larger than those in the along-wind direction. This is because the aerodynamic loading on a tall building usually results from the atmospheric turbulence and wake excitation due to vortex shedding. The atmospheric turbulence in the approach flow causes fluctuating along-wind loading and wake excitation induces fluctuating across-wind loads. One can see also that all of the responses (rms-displacements and rms-accelerations) in the along-wind (angles $90deg$, $270deg$, and vicinities) and across-wind (angles $0deg$, $180deg$, $360deg$, and vicinities) of y-direction are much higher than those in the along-wind (angles $0deg$, $180deg$, $360deg$, and vicinities) and across-wind (angles $90deg$, $270deg$, and vicinities) of the x-direction respectively. This is because the contribution of the torsional response to the overall response in

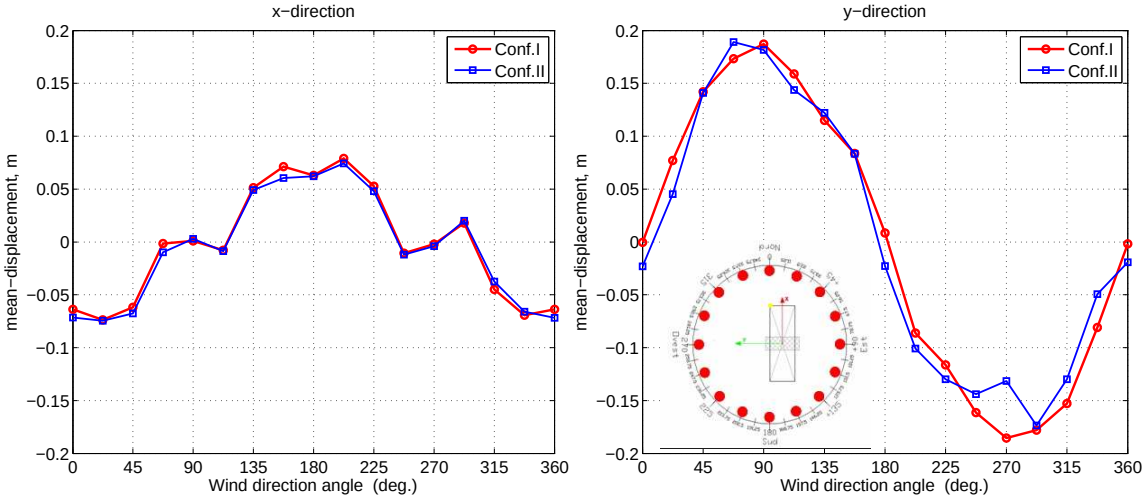

Figure 14: Mean displacements of the top corner in x and y-directions.

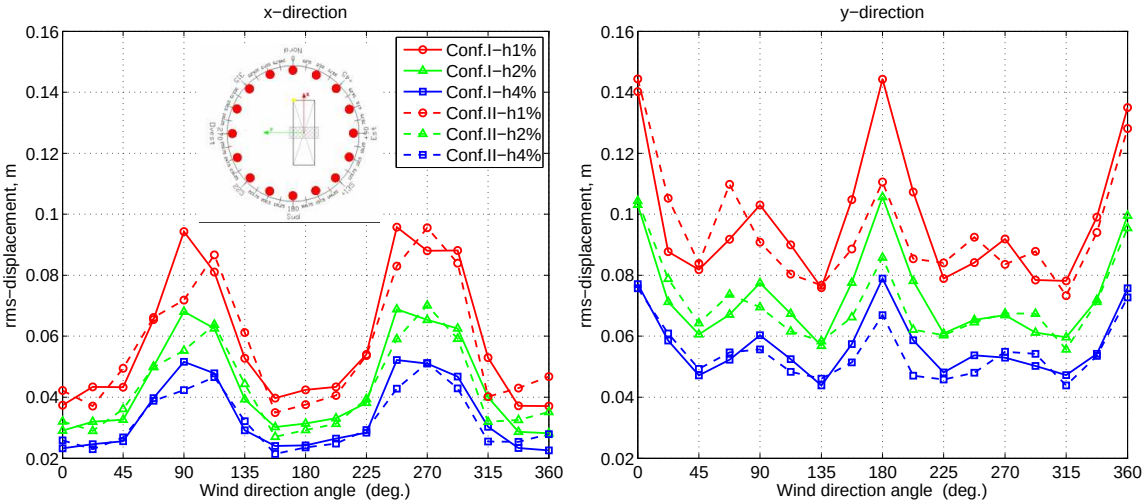

Figure 15: RMS displacements of the top corner in x and y-directions.

the y-direction is about 2.56 times the contribution of the torsional response in the x-direction (the building has a rectangular cross-section). Also, this is due to the unequal effects of the flow around the prism.

One can see from Figs. (15-16), for the responses under Config. I, that the effect of low rise buildings in the surrounding result in an increase in the along-wind response (responses in the y-direction at angle $90deg$ are higher than those at angle $270deg$) but reduction in the across-wind response (responses in the x-direction at angle $90deg$ are slightly lower than those at angle $257.5deg$) when they exist in the upstream wind (see Fig. 8). This means that short buildings perform like roughness elements in the upstream wind and increase the turbulence of the upcoming wind which increases the along wind response; while the increased along-wind turbulence decreases the across-wind responses. This reveal an important fact, i.e., the dynamic responses for the along-wind direction increases with the increase in the turbulence intensity.

The interference effect of the tallest building in the surroundings which generally has building height about 80% of the tower resulted into a reduction in the mean along-wind displacement responses in the y-direction when the tower was partially covered by this building (angle

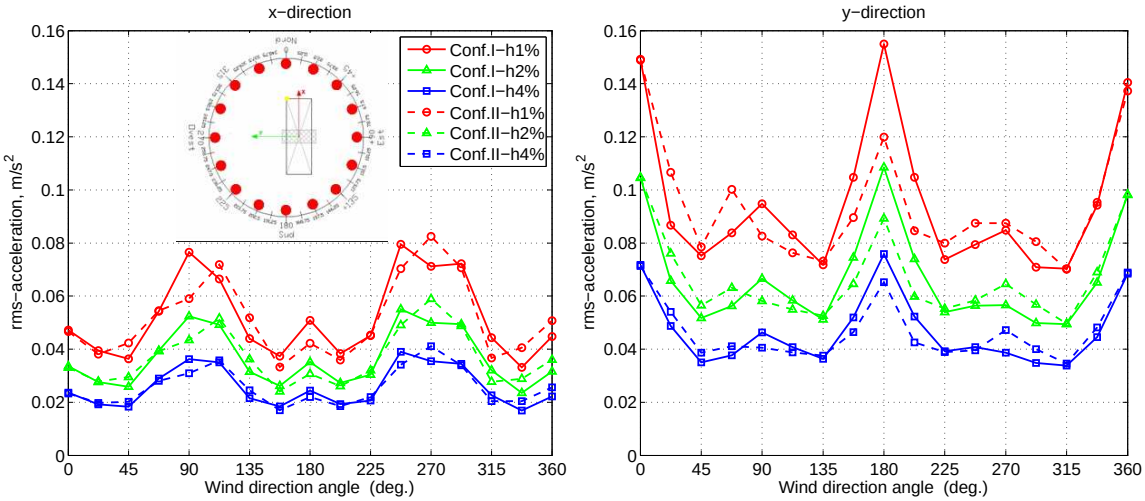

Figure 16: RMS accelerations of the top corner in x and y-directions.

$270deg$ (see also Fig. 12)). However, this interference has no significant reduction on the rms responses which mainly depend on the fluctuating component of the wind load.

Figures (15-16) with Fig. 8-(b)) indicates that the across-wind responses in the y-direction (angle $180deg$) are highly decreased due to the turbulence generated behind a building in the surrounding when it exist in the upcoming wind (this build-ing has a height of about 50% of the towers height).

7 DAMPING EFFECTS

In order to estimate the damping level necessary for comfort purposes, numerical simulation with different damping ratios, h, were conducted. Three levels were tested: $h = 1\%$, $h = 2\%$ and $h = 4\%$.

7.1 Expecting damping effects

Considering SDOF mechanical system forced by a simple harmonic resonant input ($\Omega = \omega_0$), the response is again simple harmonic. Now, if damping is doubled($h = 1\% \rightarrow h = 2\%$), its response, so its RMS, will reduce by a factor 0.707, [15].

If the system is forced by a white noise excitation $F(\Omega = \omega_0)$, the response will be composed by static and a narrow-band resonant response, Eq. (7).

$$\frac{X_0}{X_{st}} = S\left(\frac{\Omega}{\omega_0}; h\right) = \frac{1}{1 - \left(\frac{\Omega}{\omega_0}\right)^2 + i2h\frac{\Omega}{\omega_0}} \tag{7}$$

The RMS of the response, given by Eq. (8), is then the RMS of the function in Eq. (7) short of $F(\Omega = \omega_0)$.

$$RMS\,(h) = \left(X_{st} \frac{1}{\overline{\Omega/\omega_0}} \int_0^{\overline{\Omega/\omega_0}} \frac{1}{\left(1 - \left(\frac{\Omega}{\omega_0}\right)^2\right)^2 + \left(2h\frac{\Omega}{\omega_0}\right)^2} d\left(\frac{\Omega}{\omega_0}\right) \right)^{0.5} \tag{8}$$

If the damping ratio of the mechanical system is small, Fig. 17, the resonant peak gives quite all the contribution to the RMS. In this case it can be shown that, Eq. (9), [15]:

$$\frac{RMS\left(h_2\right)}{RMS\left(h_1\right)} = \left(\frac{\overline{\left|S\left(\frac{\Omega}{\omega_0};h_2\right)\right|^2}}{\overline{\left|S\left(\frac{\Omega}{\omega_0};h_1\right)\right|^2}} \right)^{0.5} \simeq \left(\frac{h_1}{h_2}\right)^{0.5} \tag{9}$$

This means that if the amount of damping is being double, the RMS reduction is so reduced by a factor $1/\sqrt{2}$. However, in order to have a reduction in the response of 50%, it is necessary to have the damping ratio multiply by four.

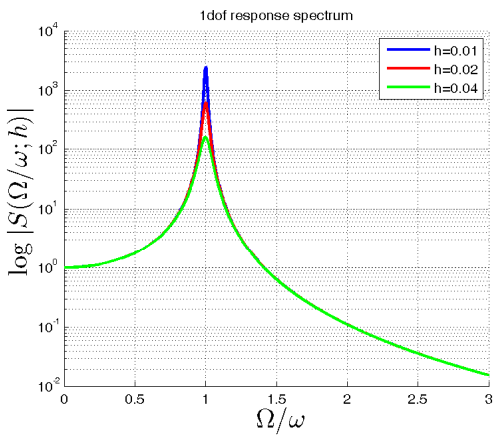

(a) Response of SDOF

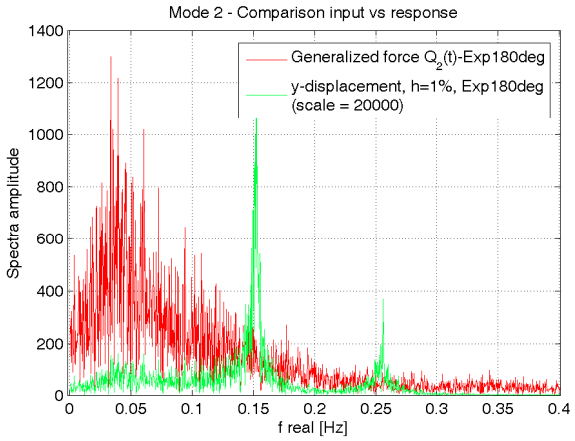

(b) Generalized force Q_{II} and tower response amplitude spectra.

Figure 17: Role of the damping on the response

The wind, and so the generalized force spectrum, carried at the real using the equality on the reduced frequencies, Eq. (10),

$$\left[\frac{f \cdot L}{V}\right]_M = \left[\frac{f \cdot L}{V}\right]_R \rightarrow \lambda_f = \frac{\lambda_V}{\lambda_L} \tag{10}$$

has the largest energy content in a band frequency lower than the building natural frequencies (Fig. 17(b)): it is then like a white noise spectrum in the resonant region of the building response.

7.2 Results of the simulations

Figures (15 - 16) and Table 1 for the exposure angle 360 deg, show that the RMS response dependence on damping obtained from the numerical simulations is in agreement with the expected results: doubling the damping ratio, the RMS simulated response is reduced by a factor of about 0.7. In order to reduce displacements and accelerations by 50%, the damping must be multiply by four.

Figures (15-16) show that damping is effective in reducing rms responses under the two configurations. However, for comfort reasons, rms-accelerations are limited to be lower than 0.06 m/s2 [17] for this specific building under the current study conditions (wind has a return period of 5 years and the wind speed is assumed to be constant for all of the wind attack angles).

Exp. angle (deg)	Damping (%)	Mean y-displ. (m)	rms y-displ. (m)	rms y-acc. (m/s2)
360	1	-0.0017	0.135	0.1404
360	2	-0.0017	0.0995	0.0983
360	4	-0.0017	0.0757	0.0684
360	h_2/h_1	1	0.73	0.70
360	h_4/h_1	1	0.56	0.48

Table 1: Damping role on the rms responses

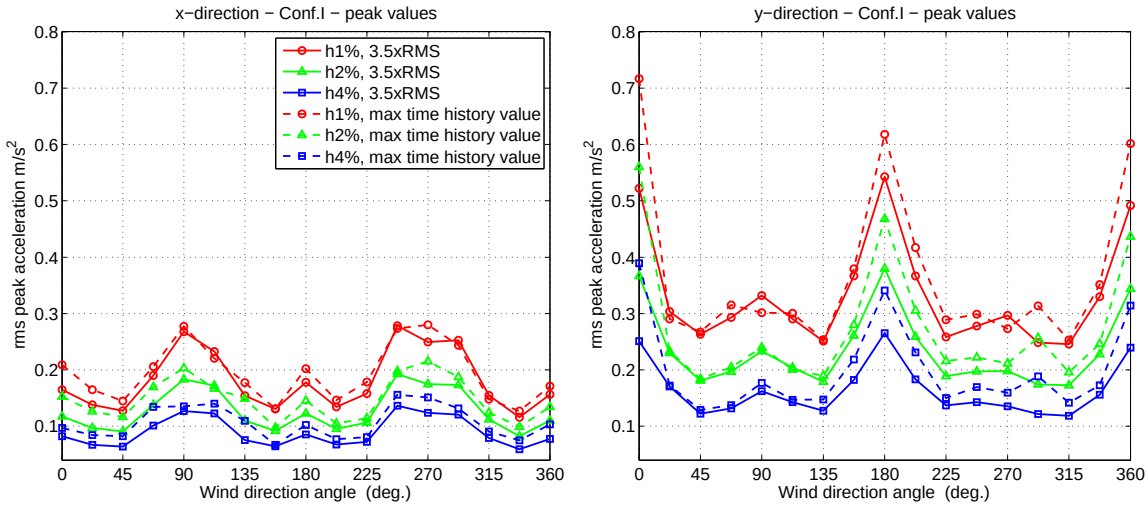

Figure 18: Peak accelerations of the top corner.

Figure (16) shows that 2% damping in the x-direction is enough to reach the comfort criteria over all of the wind attack angles while 4% damping in the y-direction still not enough to reach the comfort criteria under across wind loads. This means that a simple tuned mass damper can be used to damp the structural vibrations in the x-direction while active control is needed to damp the vibrations in the y-direction.

7.3 Evaluation of the peak

Peak accelerations, needed for the comfort verification, can be evaluated as $3.5 \times RMS$, [18]. Figure 18 show the comparison between these peaks and the maximum values obtained from the simulated time history for under Conf. I. As one can see the agreement is good. However, there are some peak values obtained from the time history that are greater than those obtained from the rms values. The analysis of the data shows that the cause of these differences is due to some isolated singular peaks in the time history, due to a transient in the input (the generalized force) perfectly resonant. As an example, Fig. 19(a) shows the generalized force of the second mode, $Q_{II}(t)$. In order to evaluate the resonant component, a band-pass filter $0.14 - 0.15$ Hz was used: from time 2960 s, one can see that the $Q_{II}(t)$ presents two resonant cycle, after that there isn't no more correlation. The displacement response in y-direction derived from this input is shown in Fig. 19(b): it is clear that the four resonant peaks of the $Q_{II}(t)$ are the cause of the peaks in the time history, highlighted in box1. It is also clear that this is a resonant condition because a negligible dependence of the transient peak response on the damping ratio h. In a

non-resonant condition, box2, it is clear that the damping reduces the response. However it is

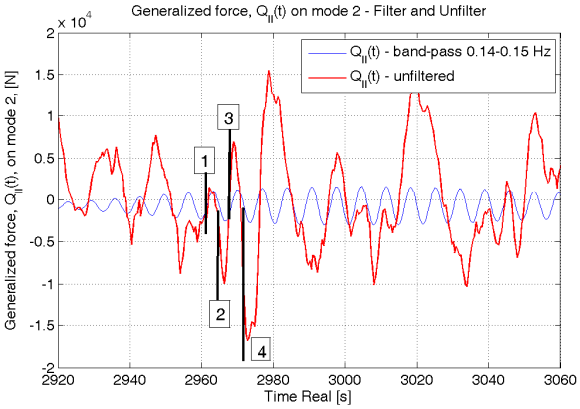

(a) Generalized force of the second mode (filtered and unfiltered)

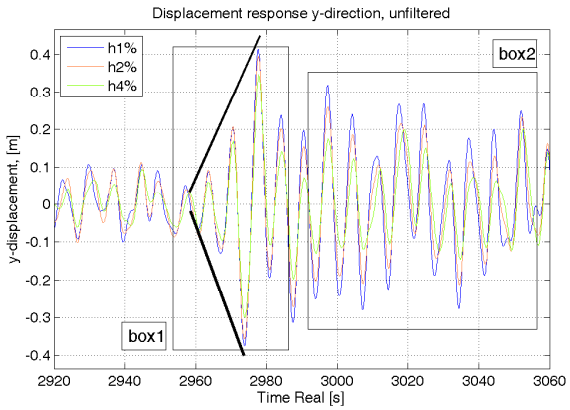

(b) Displacement response in the y-direction (unfiltered).

Figure 19: Evaluation of the peaks in the response.

believed that this behavior has a very low probability of expectation. If no statistical regression on peaks population is allowed, reliable peaks values can be estimated from the RMS simulated response, as $3.5 \times RMS$.

8 CONCLUSIONS

Both 2D sectional and 3D rigid models were used to further the understanding of the wind flow effects around a tall building with the outer shape that is close to a rectangular prism. The 2D sectional model indicated sensitivity to galloping instability at low turbulence over critical wind attack angles ($-5deg < \alpha < +5deg$). The same phenomenon was seen again with the 3D model at low turbulence. However, such instability disappeared at higher turbulence. This is a key point that should be taken into account for the design of such structures in environments where low turbulence flow is expected.

The aerodynamic loads acting on the building are utilized with a FEM of the building to predict its dynamic responses under wind loads. This approach has the advantage of combining along-wind, across-wind and torsional responses altogether. The technique used allows for considering higher modes of vibration. The effect of the wind incident angle is very important as the highest values of the displacement and acceleration responses may occur at angles rather than $0deg$ or $90deg$ (at which it is difficult to calculate such responses using traditional codes). At the same turbulence intensity, responses in the across-wind direction are larger than those in the along-wind direction. This reveals the importance of the technique proposed as many codes provide details to calculate the along-wind response but not the across-wind and torsional responses. The existence of short buildings in front of the tower enhances the turbulence which results in an increase in the along-wind responses but a general decrease in the across-wind responses. The effect of the interference of the surrounding tall buildings (which have generally heights of about 80% of the tower) has a general effect of a reduction in the mean along-wind displacement if the wind is coming from their direction.

Damping was seen to be effective in reducing the responses of the tower in order to reach the design comfort level. It is shown that the tower requires much damping in one lateral direction than the other which is due to the unequal effects of the flow around the building and

the contribution of torsion. However, the procedure developed permits the displacement and acceleration levels of tall buildings to be estimated at the preliminary design stages.

9 ACKNOWLEDGEMENTS

The help offered by the staff of the wind tunnel and many volunteers who did share in setting up the experimental work is really appreciated.

REFERENCES

[1] American society of civil engineers. *Minimum design loads for buildings and other structures*. SEI/ASCE 7-02, Reston, Virginia, 2008.

[2] Eurocode 1. *Actions on structures - Part 1-4: General actions - Wind actions*. prEN 1991-1-4, European Standard, 2004.

[3] A. Kareem. Dynamic Response of High-Rise Buildings to Stochastic Wind Loads. *Journal of Wind Engineering and Industrial Aerodynamics*, **42(1-3)**, 1101-1112, 1992.

[4] A. Kareem. Aerodynamic Response of Structures with Parametric Uncertainties.*Structural Safety*, **5(3)**, 205-225, 1998.

[5] Y. Zhou, M. Gu, H. Xiang. Alongwind static equivalent wind loads and responses of tall buildings. Part I: Unfavorable distributions of static equivalent wind loads. *Journal of Wind Engineering and Industrial Aerodynamics*, **79(1-2)**, 135-150, 1999.

[6] Y. Zhou, M. Gu and A. Kareem. Stochastic Wind-Excited Response of Tall Buildings: Influence of Mode Shapes. *In: Proceedings of the 8th ASCE Joint Specialty Conference on Probabilistic Mechanics and Structural Reliability*, Notre Dame, Indiana, July 24-26, 2000.

[7] NatHaz. *Aerodynamic Loads Database*, http://aerodata.ce.nd.edu/, 2008.

[8] A.M. Aly, A. Zasso and F. Resta. Pressure Integration Technique for Predicting Wind-Induced Response of a High-Rise Building. Paper submitted to *Journal of Wind Engineering and Industrial Aerodynamics*, 2007.

[9] O. Tietjens and G. Prandtl. *Applied Hydro and Aeromechanics*. Editor: McGraw-Hill, New York, 1934.

[10] E. Simiu and R. Scanlan. *Wind effects on structures*. Editor: John Wiley & Sons, New York, 1996.

[11] R.P. Hoxey et al. Observations of Reynolds number sensitivity in the separated flow region on a bluff body. *Journal of Wind Engineering and Industrial Aerodynamics*, **73(3)**, 231-249, 1998.

[12] G.L. Larose and A. D'Auteuil. On the Reynolds number sensitivity of the aerodynamics of bluff bodies with sharp edges. *Journal of Wind Engineering and Industrial Aerodynamics*, **94(5)**, 365-376, 2006.

[13] K. Shimada, T. Ishihara. Prediction of aeroelastic vibration of rectangular cylinders by k-epsilon model. *Journal of Aerospace Engineering*, **12(4)**, 122-135, 1999.

[14] P. Hémon and F. Santi. On the aeroelastic behaviour of rectangular cylinders in cross-flow. *Journal of Fluids and Structures*, **16(7)**, 855-889, 2002.

[15] G. Diana and F. Cheli. *Dinamica e vibrazione dei sistemi*. Editor: Utet, Torino, 1993.

[16] L. Rosa. *Studio in galleria del vento del comportamento aerodinamico ed aeroelastico di un alto edificio a torre a sezione rettangolare*. Ph.D. thesis, Dipartimento di Meccanica, Politecnico di Milano, Italy, 2008.

[17] ISO 6897-1984 (EI) *Guidelines for the evaluation of the response of occupants of fixed structures, especially buildings and off-shore structures, to low-frequency horizontal motion (0,063 to 1 Hz)*. International Organization for Standardization, 1984.

[18] K.C.S. Kwok. *Motion simulator study on effects of wind-excited tall building motion on occupants*. Presented at Wind effects on buildings and urban environment, Tokio, Japan, 2008.